Novel Solar Sail Mission Concepts for High-Latitude Earth and Lunar Observation

Heiligers, Jeannette; Parker, Jeffrey S.; Macdonald, Malcolm

DOI
10.2514/6.2016-5373

Publication date
2016

Document Version
Accepted author manuscript

Published in
AIAA/AAS Astrodynamics Specialist Conference

Novel Solar Sail Mission Concepts for High-Latitude Earth and Lunar Observation

Jeannette Heiligers[1]
Delft University of Technology, 2629 HS Delft, the Netherlands
University of Colorado, Boulder, CO 80309, USA

Jeffrey S. Parker[2]
University of Colorado, Boulder, CO 80309, USA

and

Malcolm Macdonald[3]
University of Strathclyde, Glasgow G1 1XJ, Glasgow, United Kingdom

This paper proposes the use of solar sail periodic orbits in the Earth-Moon system for observation of the high-latitudes of the Earth and Moon. At the Earth, the high-latitudes will be crucial in answering questions concerning global climate change, monitoring space weather events and ensuring sustainable development of these fragile regions. The polar regions of the Moon, especially the South Pole, are of great scientific interest as well as a potential destination for a future permanent lunar base. The existence of families of solar sail periodic orbits in the Earth-Moon system has previously been demonstrated by the authors and is expanded in this paper by introducing additional orbit families. The paper focuses in particular on orbits that are achievable with near-term solar sail technology and that originate by maintaining the solar sail at a constant attitude with respect to the Sun such that mission operations are greatly simplified. The results provide a set of constellations for continuous observation of the high-latitudes. For example, a constellation of two solar sail L_2-displaced vertical Lyapunov orbits can achieve continuous observation of both the lunar South Pole and the center of the Aitken Basin at a minimum elevation of 15 deg, while at the Earth, a set of two, so-called 'clover-shaped' orbits can provide continuous coverage of one of the Earth's Poles at 20 deg minimum elevation. Transferring these orbits to a higher-fidelity model, taking among others the eccentricity of the Moon into account, shows that these orbits still exist without any significant impact on their performance for high-latitude observation of the Earth and Moon.

---

[1] Marie Curie Research Fellow, Faculty of Aerospace Engineering, Kluyverweg 1, and Colorado Center for Astrodynamics Research, AIAA Member.
[2] Assistant Professor, Colorado Center for Astrodynamics Research
[3] Reader, Advanced Space Concepts Laboratory, Department of Mechanical and Aerospace Engineering, AIAA Associate Fellow.

I. Introduction

The successes of the JAXA's IKAROS (2010), NASA's NanoSail-D2 (2010) and The Planetary Society's LightSail-1 (2015) missions have sparked renewed interest in solar sailing: research in the field is flourishing and more initiatives are scheduled for the future (e.g. NEA Scout (NASA) [1]). The unique selling point of solar sailing of not relying on an onboard reaction mass makes solar sailing the preferred option for a range of mission applications [2, 3]. Key mission concepts include: precessing an elliptical Earth-centred orbit for long residence times in the Earth's magnetotail (also known as the GeoSail mission concept) [4, 5][6, 7], hovering along the Sun-Earth line sunward of the L_1 point for increased warning times for space weather events (also known as the GeoStorm mission concept) [8, 9], using a sail to achieve a solar polar orbiting probe for high-latitude, close proximity observations of the Sun [5, 10], as well as more far-term concepts such as the interstellar heliopause probe where a close approach of the Sun is used for a "photon-gravity assist" which allows a rapid transit through the Solar System without the need for a heavy-lift launch vehicle or a long sequence of gravity assists [11].

The purpose of the current paper is to complement this extensive list of potential solar sail applications, specifically focusing on the sail's potential for high-latitude observation of the Earth and Moon. Continuous observation of the high-latitudes of the Earth will be crucial in on-going study of global climate change, but also to support space weather monitoring and forecasting activities, telecommunications, weather forecasting and ship navigation for the exploration and sustainable development of these regions. The polar region of significant interest as it is projected to hold 30 percent of the world's undiscovered gas and 13 percent of the world's undiscovered oil [12]. In addition, with the northern sea routes opening up, an increase in shipping activity can be expected. Regarding the Moon, the permanently shadowed craters on the lunar South Pole (especially the Aitken Basin) are of significant scientific interest and could be the future destination of a permanently occupied lunar base. Both objectives require continuous observation capabilities of the lunar South Pole and, in case of a lunar base, continuous communication with Earth.

This paper aims at achieving such continuous links with high-latitude regions through the use of solar sail periodic orbits in the Earth-Moon three-body system. These orbits can be found through the use of differential correction techniques: by perturbing classical libration point orbits such as Lyapunov, halo, vertical Lyapunov and distant retrograde orbits with a solar sail induced acceleration, entirely new families of orbits result in the Earth-Moon system parametrised by the sail's acceleration [13, 14]. Different types of families can be created depending on the steering law assumed for the solar sail. In this paper a simple law, either Sun-facing or one where the sail is pitched at a constant angle with respect to the Sun-direction, is assumed, endeavouring to keep mission operations to a minimum.

Besides adding an additional family of solar sail orbits to previous work, see Reference [13, 14], this paper also investigates, for the first time, the effect of higher-fidelity dynamics on the existence and properties of the solar sail periodic orbits presented. While previous work assumed that the ecliptic and Earth-Moon planes coincide and neglected the lunar eccentricity, this paper accounts for these effects, providing realistic solar sail trajectories by expanding the differential correction technique to a *multiple shooting* differential correction method.

II. Solar sail dynamics

Initial investigations into the families of solar sail periodic orbits in the Earth-Moon system are conducted within the framework of the circular restricted three-body problem (CR3BP) [15]. To describe the solar sail's dynamics, the synodic reference frame of Figure 1a is used as well as the traditional system of canonical units, where the Earth-Moon distance, the frame's angular velocity, ω, and the Earth-Moon system mass are normalised to 1. One sidereal lunar month is then represented by 2π and with the mass ratio $\mu = m_2/(m_1+m_2)$, the location of the Earth and Moon along the x-axis become $-\mu$ and $1-\mu$, respectively. Following Reference [2], the solar sail dynamics are then governed by the following set of equations of motion

$$\ddot{\mathbf{r}} + 2\boldsymbol{\omega}\times\dot{\mathbf{r}} = \mathbf{a}_s - \nabla U \,. \tag{1}$$

In Eq. (1), $\mathbf{r} = \begin{bmatrix} x & y & z \end{bmatrix}^T$ is the solar sail dimensionless position vector, $\boldsymbol{\omega} = \omega\hat{\mathbf{z}}$ is the synodic frame's angular velocity vector and $U = -\frac{1}{2}\left(x^2+y^2\right) - \left(\left[1-\mu\right]/r_1 + \mu/r_2\right)$ is the effective potential with the Earth-sail and Moon-sail vectors defined as $\mathbf{r}_1 = \begin{bmatrix} x+\mu & y & z \end{bmatrix}^T$ and $\mathbf{r}_2 = \begin{bmatrix} x-(1-\mu) & y & z \end{bmatrix}^T$, respectively.

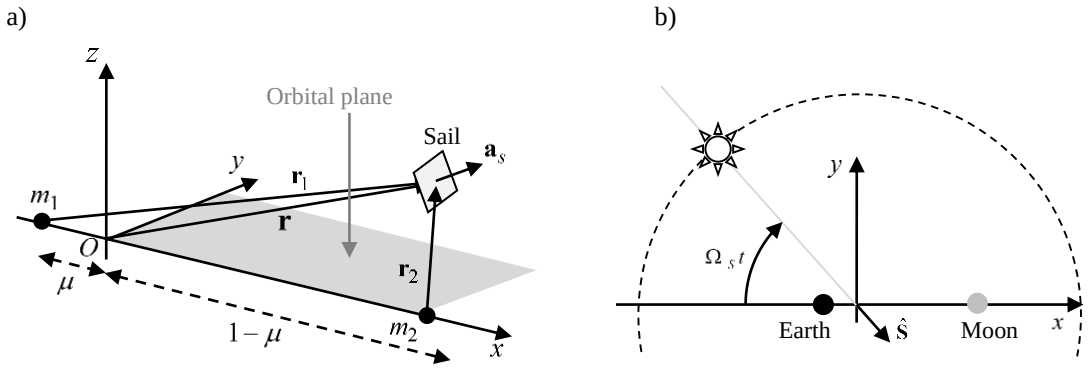

Figure 1a) Schematic of solar sail circular restricted three-body problem. b) Schematic of non-autonomous solar sail Earth-Moon three-body problem.

The term that differentiates Eq. (1) from the *classical* CR3BP dynamics is the solar sail induced acceleration, $\mathbf{a}_s$. To define this acceleration it is important to note that, when considering the synodic reference frame of Figure 1a, the Sun "orbits" around the Earth-Moon system once per synodic lunar period, see Figure 1b, and therefore the direction of the photons impacting the sail membrane changes over time, making the dynamics in Eq. (1) time dependent. In particular, the Sun-direction, $\hat{\mathbf{S}}$, can be described as $\hat{\mathbf{S}}(t) = \begin{bmatrix} \cos(\Omega_S t) & -\sin(\Omega_S t) & 0 \end{bmatrix}^T$ with $\Omega_S = 0.9252$ the Sun's orbital angular rate and t the dimensionless time. Note that the small offset between the Earth-Moon and ecliptic planes of approximately 5 deg is neglected here, but will be accounted for later on in the paper. It is furthermore important to note that this paper adopts an ideal solar sail model, according to which the solar photons are specularly reflected and the solar radiation pressure force acts perpendicular to the solar sail membrane, along the sail normal

vector $\hat{\mathbf{n}}$ [2, 3]. Note that a small tangential force component exists with more realistic sail reflectance models, but previous analyses have shown that this component has only a small effect on the sail's performance [11]. Therefore, when neglecting this tangential component, the solar sail induced acceleration can be described as

$$\mathbf{a}_s = a_{0,\mathrm{EM}} \left(\hat{\mathbf{S}}(t) \cdot \hat{\mathbf{n}} \right)^2 \hat{\mathbf{n}} . \tag{2}$$

In Eq. (2) the magnitude of the acceleration, $a_{0,\mathrm{EM}} \left(\hat{\mathbf{S}}(t) \cdot \hat{\mathbf{n}} \right)^2$, is assumed to be independent of the sail's location in the Earth-Moon system, i.e. the Sun-sail distance is assumed to be constant throughout the Earth-Moon system at 1 astronomical unit (au). Furthermore, the term $\left(\hat{\mathbf{S}}(t) \cdot \hat{\mathbf{n}} \right)^2$ takes into account that, when pitching the sail away from the Sun-direction, the sail's effective area reduces and the achievable solar sail induced acceleration reduces accordingly. In this paper, however, primarily a Sun-facing steering law will be assumed in which the sail follows the Sun's orbiting motion over time, exposing its full membrane surface to the Sun at all times, see Figure 2a. The sail normal vector is thus aligned with the Sun-direction, $\hat{\mathbf{n}} = \hat{\mathbf{S}}(t)$, which reduces Eq. (2) to

$$\mathbf{a}_s = a_{0,\mathrm{EM}} \hat{\mathbf{S}}(t) . \tag{3}$$

Note that for such a Sun-facing steering law, the tangential force component of more realistic solar sail reflectance models does not play a role, because in that case the effect of non-ideal properties of the sail would only be a reduction in the acceleration magnitude, $a_{0,\mathrm{EM}}$ [9].

Alternatively, this paper also considers an out-of-plane extension of this solar sail induced acceleration law by pitching the sail in the out-of-plane direction at an angle γ with respect to the Sun-direction, see Figure 2b. Equation (2) then becomes

$$\mathbf{a}_s = a_{0,\mathrm{EM}} \cos^2 \gamma \begin{bmatrix} \cos\gamma \cos(\Omega_S t) \\ -\cos\gamma \sin(\Omega_S t) \\ \sin\gamma \end{bmatrix} . \tag{4}$$

Note that both steering laws in Eqs. (3) and (4) can be achieved passively through a correct offset between the spacecraft's center-of-pressure and center-of-mass.

The variable $a_{0,\mathrm{EM}}$ is commonly referred to as the characteristic acceleration, i.e. the acceleration that an ideal solar sail generates when facing the Sun at 1 au [2]. A common value for this acceleration, based on near-term solar sail technology, is 0.3 mm/s^2 [5, 9], which translates into a dimensionless value of approximately $a_{0,\mathrm{EM}} = 0.1$. This paper will not consider characteristic accelerations beyond this value to show what is achievable with near-term solar sail technology.

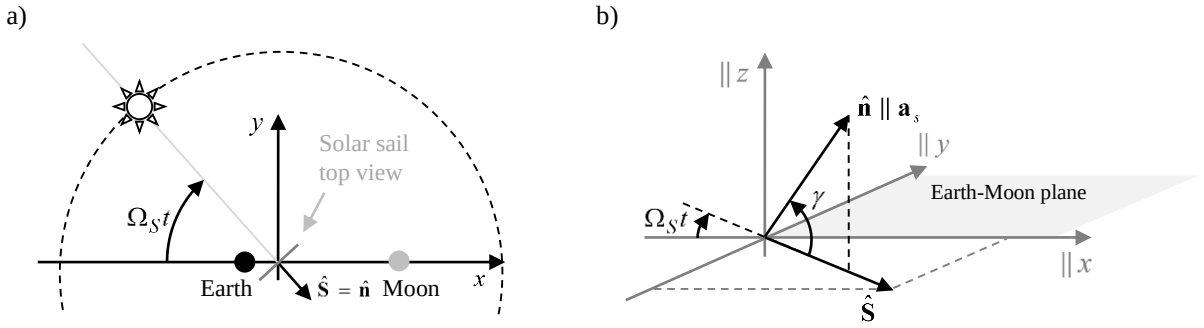

Figure 2a) Schematic of passive Sun-facing solar sail steering law b) Schematic of out-of-plane steering law.

III. Solar sail periodic orbits

To find solar sail periodic orbits under the dynamics of Eq. (1) a differential corrector scheme is applied, similar to the differential corrector schemes traditionally used to find natural periodic orbits around the libration points of the classical CR3BP [16]. These schemes rely on the use of a state transition matrix to iteratively find the initial conditions that lead to periodic motion. Furthermore, the eigenvalues of the state transition matrix can be used to derive the linear stability properties of these orbits. However, the differential corrector scheme used here differs from the one presented in Reference [16] in two respects: first, due to the system's time dependency through the continuously changing Sun-direction, $\hat{\mathbf{S}}(t)$, orbits are only repeatable over time (and thus periodic) if the period of the orbit coincides with the Sun's orbital motion around the Earth-Moon system. The period of any solar sail periodic orbit in the Earth-Moon system thus needs to equal $2\pi / \Omega_S$ or a multiple thereof. The authors have previously adapted the differential corrector scheme for classical orbits as described by Howell in Reference [16] to include a constraint such that the period is indeed driven towards a value of $2\pi / \Omega_S$ [17]. This constraint then also provides an additional equation to solve for one of the unknown initial states, which leads to the second main difference: while the differential corrector scheme for classical orbits requires one of the unknown initial states to be fixed, the addition of the periodicity constraint allows all initial states to be free. This is important as it cannot be known *a priori* where (i.e., for which value of any of the initial states) solar sail periodic orbits will exist in the Earth-Moon system. For details on the adapted differential corrector scheme, the reader is referred to Reference [14].

To seed the differential corrector, a continuation scheme is applied where a classical periodic orbit is used as the very first initial guess for a very low value for the solar sail characteristic acceleration and where the result of that run is used as initial guess for a slightly larger solar sail characteristic acceleration value. By continuing this process up to a maximum value for the characteristic acceleration of $a_{0,\mathrm{EM}} = 0.1$, families of solar sail periodic orbits in the Earth-Moon system arise for increasing sail performance. Note that the classical orbit used for the very first step in the continuation scheme is chosen such that it has a period already coinciding with a desired fraction of the required period of the solar sail orbits of $2\pi / \Omega_S$.

Two example families are shown in Figure 3 and Figure 4, which will later be exploited for high-latitude observation of the Earth and Moon. The family shown in Figure 3 is coined the family of 'clover-shaped' orbits after the shape of its projection onto the (x, y)-plane. These orbits originate from using the steering law in Eq. (3) in a continuation on the value for $a_{0,\mathrm{EM}}$ (colours in Figure 3a-d) starting from a classical, highly-elliptically shaped Earth-centred orbit with a period of half the synodic lunar month. As this classical orbit passes through the Earth, see Figure 3b, it is of no practical use, but as Figure 3 demonstrates, adding a solar sail induced acceleration can move this orbit away from the Earth's center. The stability of the orbit family is presented in Figure 3e through the value of the largest eigenvalue, $\|\lambda\|_{\max}$, of the monodromy matrix (the state transition matrix evaluated after one full orbit). An orbit is stable if all six eigenvalues lie on the unit circle, i.e. $\|\lambda\|_{\max} = 1$. If the norm of any of the eigenvalues is larger than one, the orbit is unstable, with larger norm values indicating greater instability. Figure 3e shows that for the solar sail characteristic acceleration magnitudes considered in this paper ($a_{0,\mathrm{EM}} \leq 0.1$) the orbits are slightly unstable, but that they become stable for larger acceleration magnitudes.

The second family, in Figure 4, is an example of a family of solar sail vertical Lyapunov orbits at the L_2 point. This family originates from using the steering law in Eq. (4) with $\gamma =$ -35.26 deg in a continuation starting from a classical vertical Lyapunov orbit with a period of two-thirds of the synodic lunar month. The value for γ of -35.26 is selected because it is known to give the maximum out-of-plane acceleration component [2] and the minus sign ensures that the acceleration is directed below the Earth-Moon plane, which will become of importance when investigating these orbits for coverage of the southern hemisphere of the Moon, see Section IV.B.

Through the use of an out-of-plane steering law, the orbits are slightly displaced in the out-of-plane direction, pulling them below the lunar South Pole. Although all solar sail vertical Lyapunov orbits are highly unstable, see Figure 4e, the solar sail does have a small stabilizing effect as the maximum eigenvalue norm decreases (up to an order of magnitude) for increasing values for $a_{0,\mathrm{EM}}$.

Finally, note that, because of the symmetry of the problem, all orbits presented in this section can be mirrored in the (x, y)-plane.

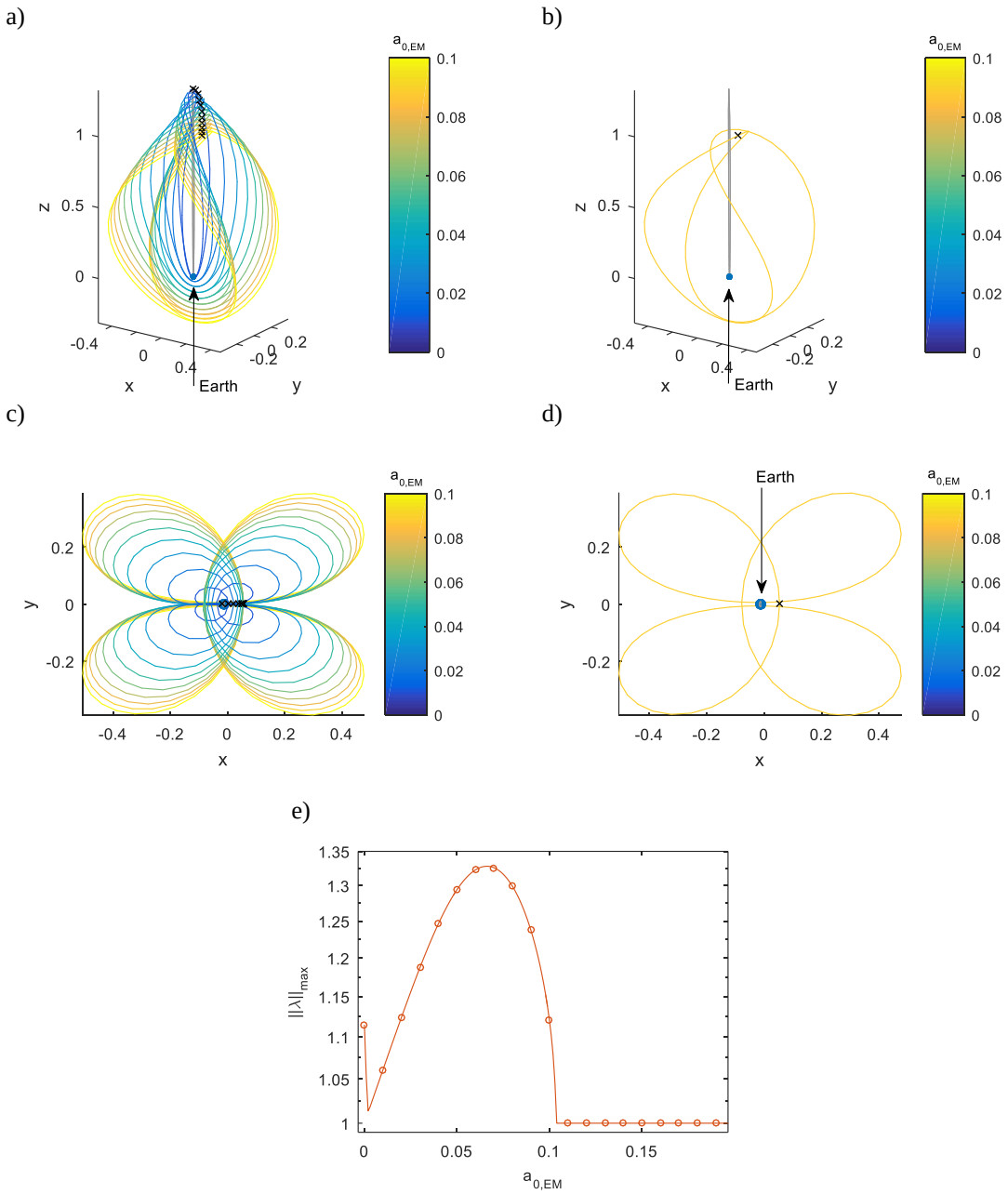

Figure 3 Solar sail Earth-centred clover-shaped orbits. Crosses indicate the initial condition. a,c) Family of orbits for increasing $a_{0,EM}$. b,d) Orbit for $a_{0,EM}$ = 0 and $a_{0,EM}$ = 0.1. e) Linear stability.

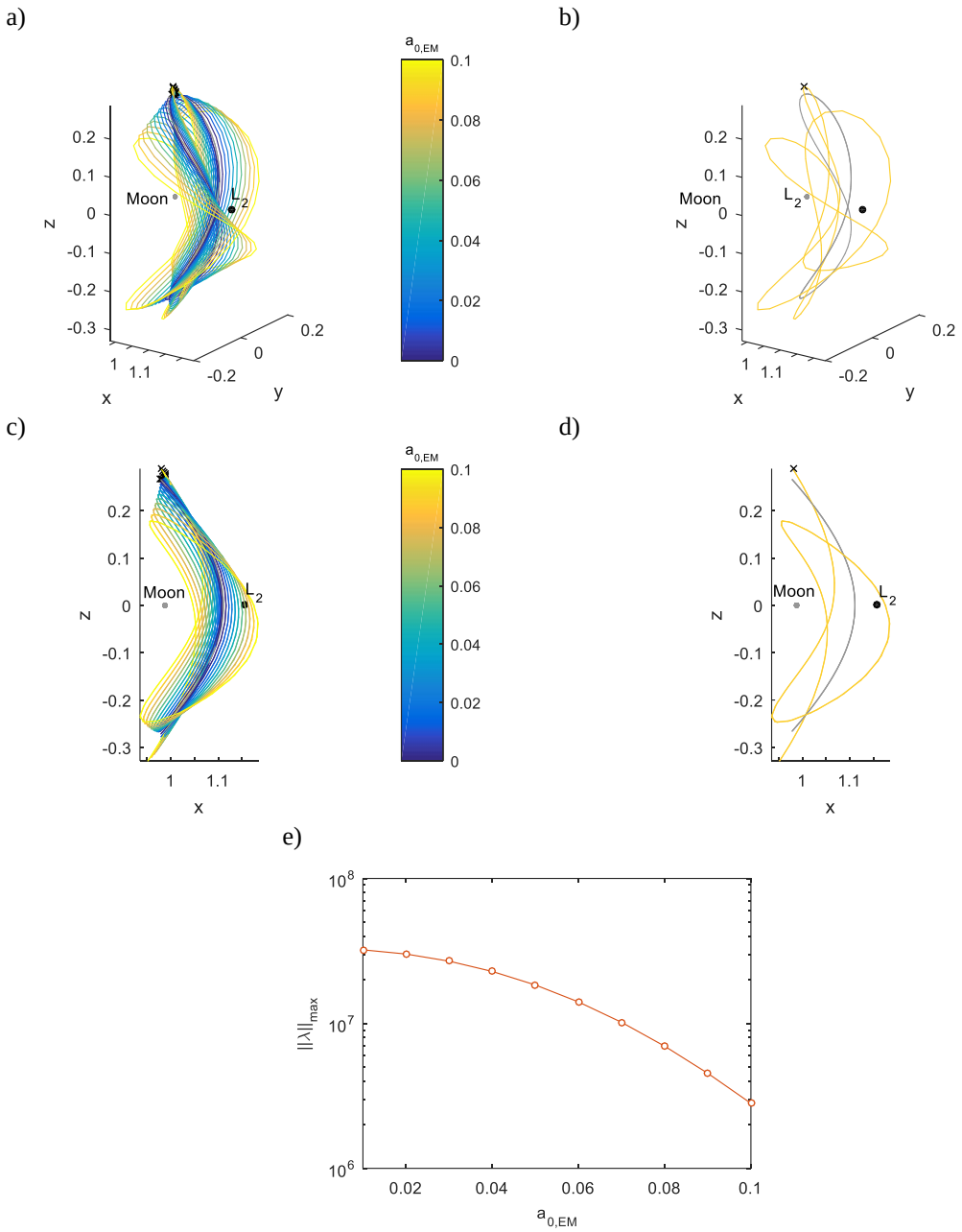

Figure 4 Solar sail L_2 vertical Lyapunov orbits. Crosses indicate the initial condition. a,c) Family of orbits for increasing $a_{0,EM}$. b,d) Orbit for $a_{0,EM} = 0$ and $a_{0,EM} = 0.1$. e) Linear stability.

IV. High-latitude observation analyses

The objective of this section is to show how a subset of orbits presented in Figure 3 and Figure 4 can achieve (near-)continuous observation of the high-latitudes of the Earth and Moon. This is done by computing the spacecraft's elevation, ε, over time at locations on Earth separated by 1 deg in latitude, and longitude. The metric used is the

amount of time that the spacecraft is above a minimum elevation, $\varepsilon \geq \varepsilon_{\lim}$. This is expressed as the 'percentage coverage', i.e. the percentage of time over a full year or a full orbital period that the condition $\varepsilon \geq \varepsilon_{\lim}$ is satisfied at a particular location or latitude of the Earth or Moon.

A. Clover-shaped orbits for Earth observation

Observation of the high-latitudes of the Earth can be achieved with satellites in low-altitude, high-inclination orbits such as the ICESat-1 (NASA, 2003- 2010) and Cryosat-2 (ESA, 2010 – ongoing) missions. Although enabling high spatial resolution observations, the low-altitude of the polar orbits restricts spacecraft to observe only narrow swaths of the polar regions during each passage. For example, CryoSat repeats it ground track only after 369 days, with a sub-cycle of 33 days, only after which uniform coverage of the polar regions is obtained. Higher temporal resolution can be achieved from Molniya orbits, but satisfactory coverage of the polar caps or high-latitude regions cannot always be achieved. In addition to these traditional concepts, the literature shows a range of other concepts for high-latitude observation, including Taranis orbits [18], pole-sitter orbits [19], solar sail displaced equilibria [20] and eight-shaped orbits [21] in the Sun-Earth system, all providing a different trade-off between resolution of the observations (i.e. distance from Earth), number of spacecraft required for continuous coverage and required propulsion technology (if any). The purpose of the current work is to complement these concepts with the capabilities provided by the clover-shaped orbits of Figure 3. These orbits are closer to Earth than previously proposed solar sail concepts such as the pole-sitter orbits and displaced equilibria and require fewer satellites for continuous coverage than constellations in low-altitude orbits, as will be shown below.

As mentioned, the percentage of time that the condition $\varepsilon \geq \varepsilon_{\lim}$ is satisfied is used as the metric to express the high-latitude coverage from the clover-shaped orbits. It will be clear from the orbital plots in Figure 3 that one spacecraft cannot provide continuous coverage of these high-latitudes as it will 'dip' below the Earth for short periods of time during the orbit. A constellation of two spacecraft will thus be required, where one of the orbits is mirrored in the (x, y)-plane. To find out which constellation would perform best, a grid search is performed over the choice for the characteristic acceleration for both orbits, computing the temporal coverage with a minimum elevation angle of $\varepsilon_{\lim} = 27$ deg for each constellation. This value for $\varepsilon_{\lim}$ reflects the elevation of a geostationary spacecraft at a latitude of 55 deg above which the accessibility of geostationary spacecraft for Earth observation applications is not assured. When considering a minimum required elevation of $\varepsilon_{\lim} = 27$ deg, the results as in Figure 8 can be obtained. Four different cases are considered, i.e. the coverage of the North and South Poles and the coverage of the 55 deg latitude band and Arctic circle (latitude of 66.56083 deg) averaged over the longitude. The horizontal and vertical axes show the dimensionless acceleration of the sailcraft in the two orbits, where a minimum value of $a_{0,\mathrm{EM}} > 0.025$ is considered to satisfy a minimum altitude above the Earth of 10,000 km. The colours indicate the percentage of time that the spacecraft is in view of these locations at the previously mentioned minimum elevation of $\varepsilon_{\lim} = 27$ deg.

Two suggested constellations are indicated in the subplots of Figure 8 that either provide the best temporal coverage of the North Pole ('constellation 1' with orbit 1 $\rightarrow a_{0,\mathrm{EM}} = 0.025$ and orbit 2 $\rightarrow a_{0,\mathrm{EM}} = 0.1$) or the best temporal

coverage of both Poles ('constellation 2' with both orbits $a_{0,\mathrm{EM}} = 0.025$ only mirrored in the Earth-Moon plane). The percentage coverage that each constellation can achieve for the four latitudes in Figure 8 is presented in Table 1, indicating that both constellations provide $\geq$ 93.7 percent coverage of the entire (Ant)Arctic region. More details for both constellations will be provided in the next two sub-sections.

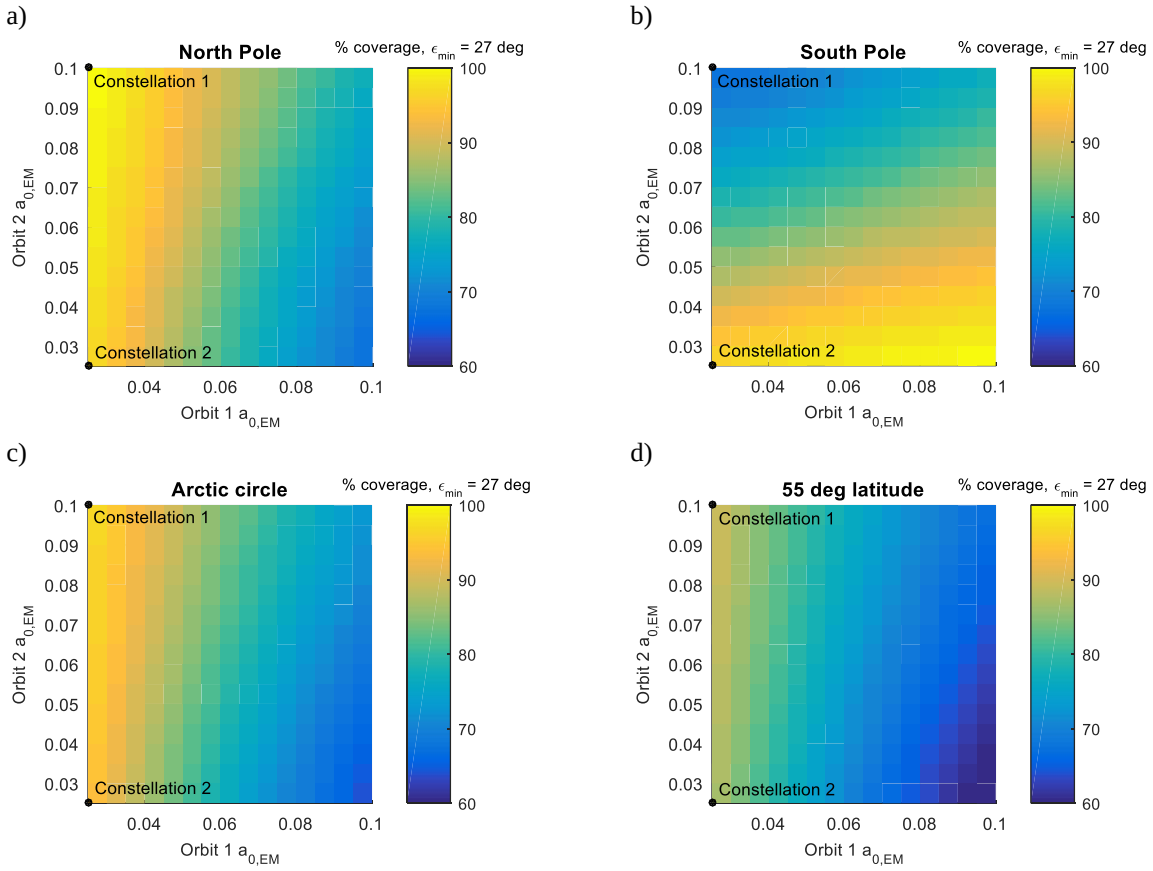

Figure 5 Percentage temporal coverage at different latitudes from clover-shaped orbits for a range of values for $a_{0,\mathrm{EM}}$. a) North Pole. b) South Pole. c) Arctic circle. d) 55 deg latitude.

Table 1 Percentage temporal coverage at different latitudes from clover-shaped orbits for constellations 1 and 2.

Latitude	Constellation 1	Constellation 2
North Pole	99.6	96.3
South Pole	66.3	96.3
Arctic circle	96.4	93.7
55 deg	89.1	86.7

Constellation 1

The first constellation, which provides near-continuous coverage (99.6 percent, see Table 1) of the North Pole (or, when mirrored in the (x, y)-plane, of the South Pole) is shown in Figure 6a, with its coverage of the North and South Poles in terms of elevation angle over time in Figure 6c and d. From the top-plot in Figure 6d it is clear that, although *continuous* coverage at $\varepsilon_{\text{lim}} = 27$ deg of the North Pole cannot be achieved from this constellation, it can be achieved when lowering the minimum elevation angle to a value of 20 deg. The coverage at lower latitudes is also provided in Table 1 with more details in Figure 7. Figure 7a provides the total useful observation time over the first orbital period. Where the lines flatten, neither of the two spacecraft is in view of the location or latitude under consideration. The actual observation time can be translated into a percentage coverage, see Figure 7b. This percentage starts at 100 percent because at the initial time the sailcraft are assumed to be at their most out-of-plane position and from this position all four locations considered in Figure 7 are in view of either spacecraft. Over time, the percentage decreases and oscillates, but after one year converges to the value as depicted in Figure 6b.

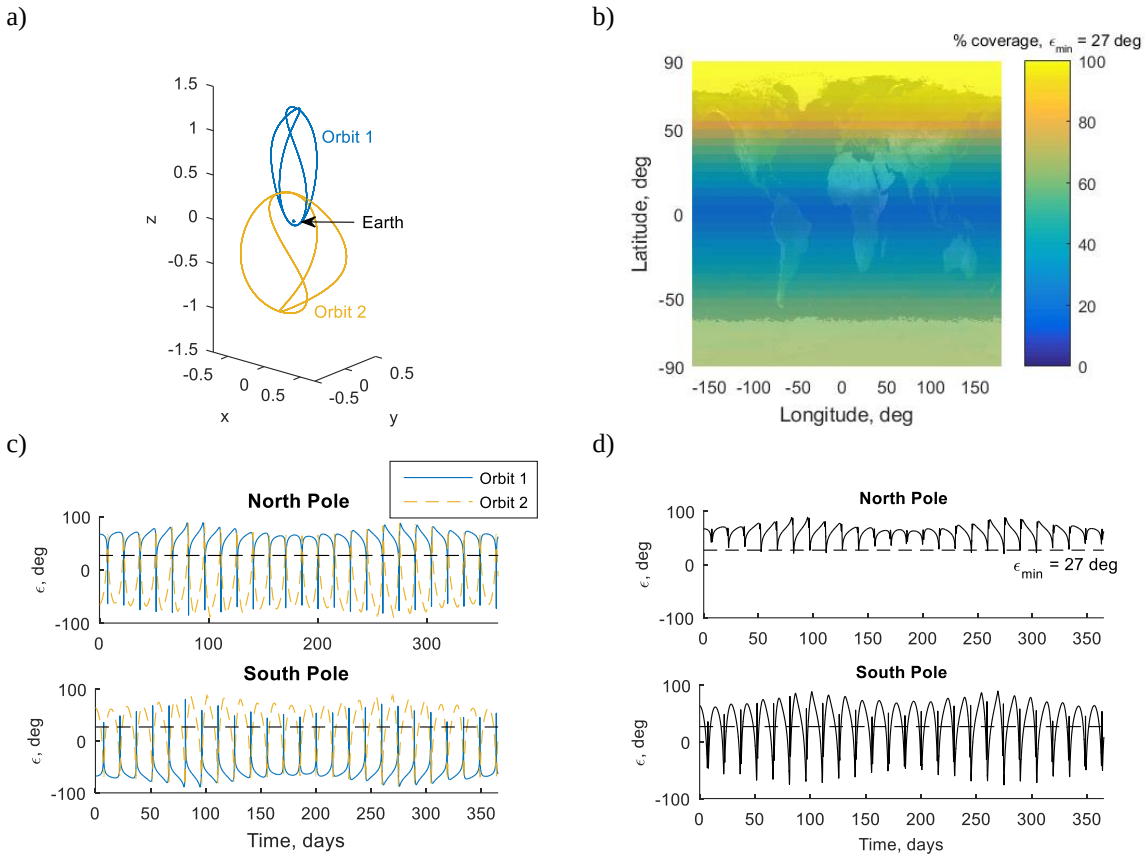

Figure 6 Clover-shaped orbits, constellation 1. a) Constellation. b) Percentage temporal coverage for minimum elevation of 27 deg. c) Elevation angle at North and South Poles for both orbits separately. d) As subplot c) but selecting best elevation angle over time.

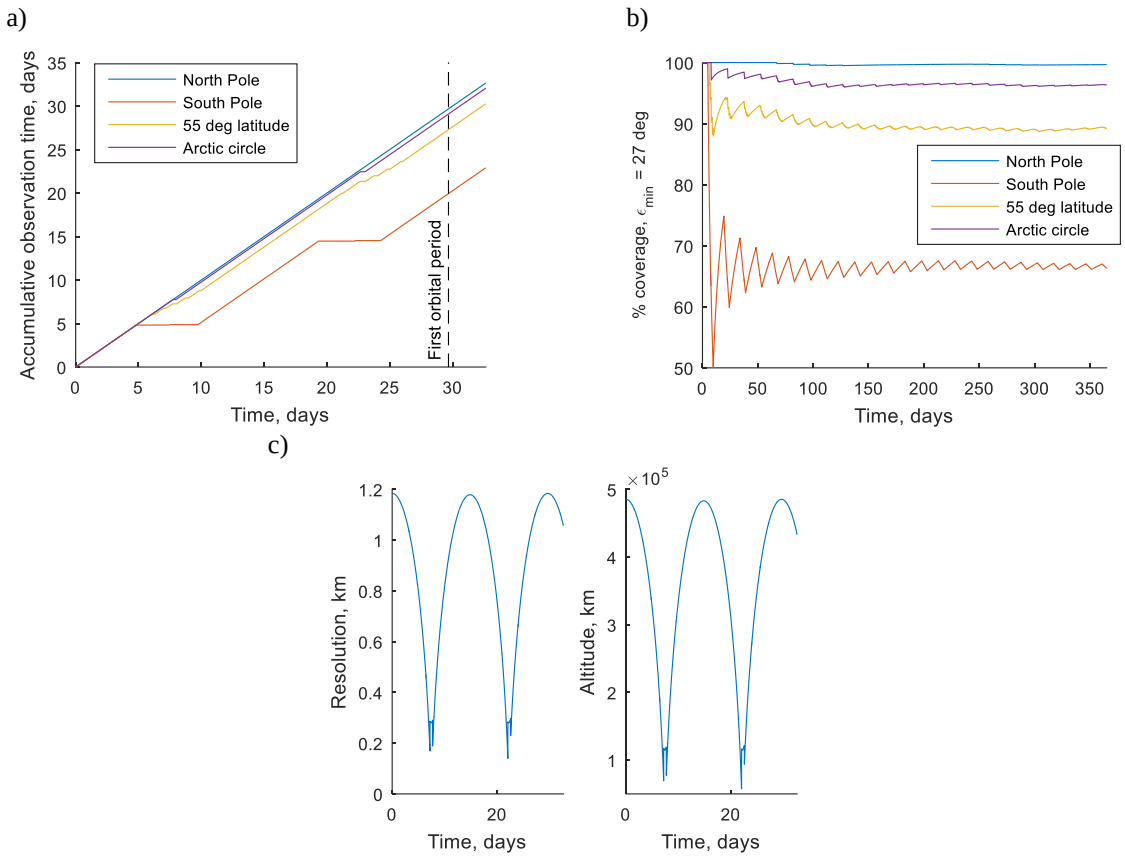

Figure 7 Clover-shaped orbits, constellation 1. a) Accumulative observation time over first orbit revolution. b) Percentage temporal coverage over time. c) Resolution and altitude (North Pole).

Finally, Figure 7c provides (for the North Pole only) information about the spatial resolution from and altitude of the constellation. The spatial resolution is computed assuming a nadir-pointing payload and that the resolution is limited by diffraction only. Under those assumptions, the resolution is a function of the observable wavelength, imager aperture diameter and orbit altitude only and scales linearly with these parameters. Because the difference in orbit altitude between the four different locations/latitudes of Figure 7a and b is very small, the results for the North Pole (as in Figure 7c) are representative for the resolution and altitude for the other three locations/latitudes. Furthermore, the results in Figure 7c are obtained assuming observations in the visible part of the spectrum (0.5 µm) and for an imager aperture diameter of 0.5 m. However, the resolution for other observations can be easily deduced from Figure 7c due to the previously mentioned linear relation: for example, for observations in the infrared part of the spectrum, the resolution increases by a factor six and for a twice as large aperture diameter the resolution decreases by a factor of two. To get an idea of more realistic performances than the diffraction limited resolution presented in Figure 7c, the EPIC camera onboard the NOAA/NASA DSCOVR mission serves as a good example. At approximately 1.5 Mkm from the Earth, this imager enables a theoretical resolution of 8 km with an effective resolution of 10-15 km (depending on the channel) at a mass of 63.2 kg (including the computer)[12]. Again assuming a linear relation between the

[1] WMO OSCAR | Details for Instrument EPIC (DSCOVR), http://www.wmo-sat.info/oscar/instruments/view/793, Accessed 24 June 2016
[2] DSCOVR: Deep Space Climate Observatory, http://www.nesdis.noaa.gov/DSCOVR/, Accessed 24 June 2016

resolution and altitude, the EPIC camera shows that a maximum spatial resolution in the order of 3-5 km should be achievable from the clover-shaped orbit constellation. Other comparisons can be made with the SEVIRI imager on the Meteosat Second Generation (MSG), which provides down to 1 km resolution in the visible spectrum[1] from geostationary orbit (GEO), and the FCI camera on the Meteosat Third Generation (MTG) which provides down to 0.5 km resolution[2] from GEO. Both imagers show that resolutions of 5-10 km should be achievable from the clover-shaped orbits.

Constellation 2

Though the constellation of Figure 6 can achieve very good coverage of one of the Poles, the coverage of the other Pole is poor (only 66.3 percent, see Table 1). Therefore constellation 2 is proposed as an alternative, see Figure 8, which consists of a mirrored constellation of two clover-shaped orbits, both with $a_{0,\mathrm{EM}} = 0.025$. Again, assuming $\varepsilon_{\mathrm{lim}} = 27$ deg this constellation achieves a coverage of 96.3 percent for *both* Poles (97.4 percent for $\varepsilon_{\mathrm{lim}} = 20$ deg) with >90 percent temporal coverage of the entire Arctic and Antarctic regions. Details, similar to the ones presented in Figure 6 and Figure 7 for constellation 1 are provided in Figure 8 and Figure 9 for constellation 2. These figures show a significant improvement in the coverage of the South Pole at similar resolution values as for constellation 1.

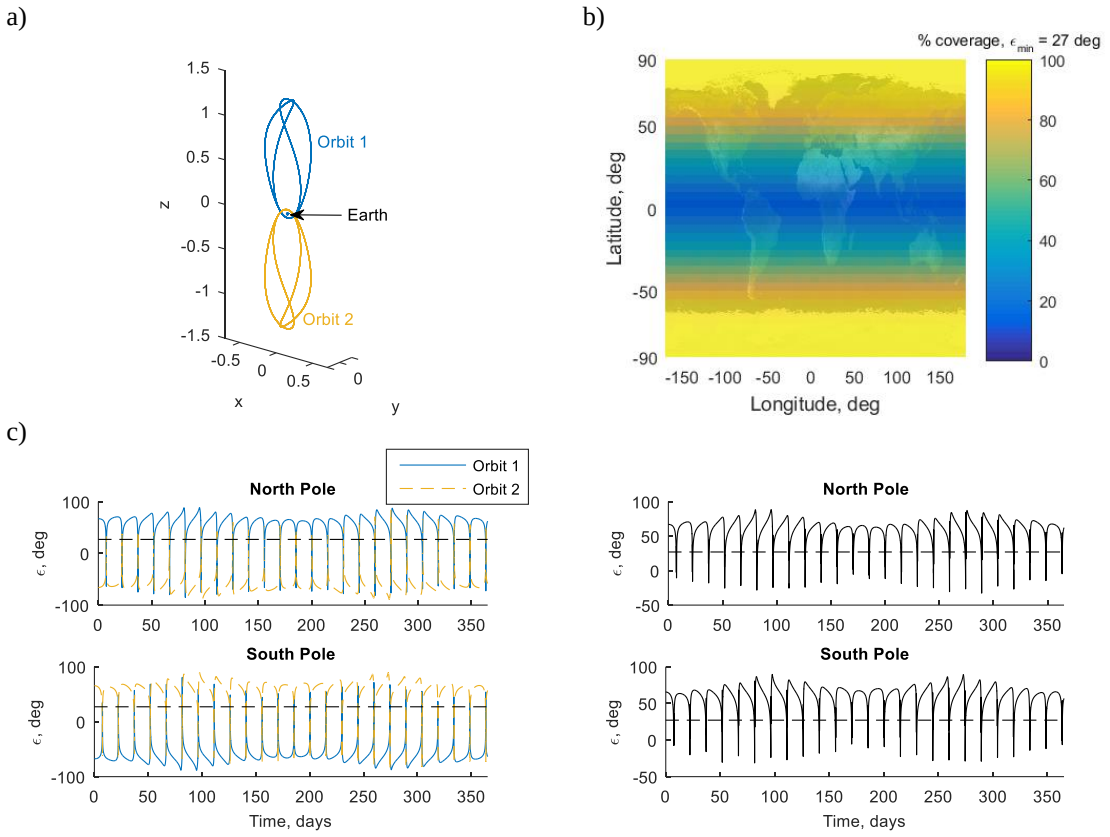

Figure 8 Clover-shaped orbits, constellation 2. a) Constellation. b) Percentage temporal coverage for minimum elevation of 27 deg. c) Elevation angle at North and South Poles for both orbits separately. d) As subplot c) but selecting best elevation angle over time.

[1] WMO: OSCAR | Details for Instrument SEVIRI, http://www.wmo-sat.info/oscar/instruments/view/503, Accessed 16 August 2016
[2] WMO: OSCAR | Details for Instrument FCI, http://www.wmo-sat.info/oscar/instruments/view/138, Accessed 16 August 2016

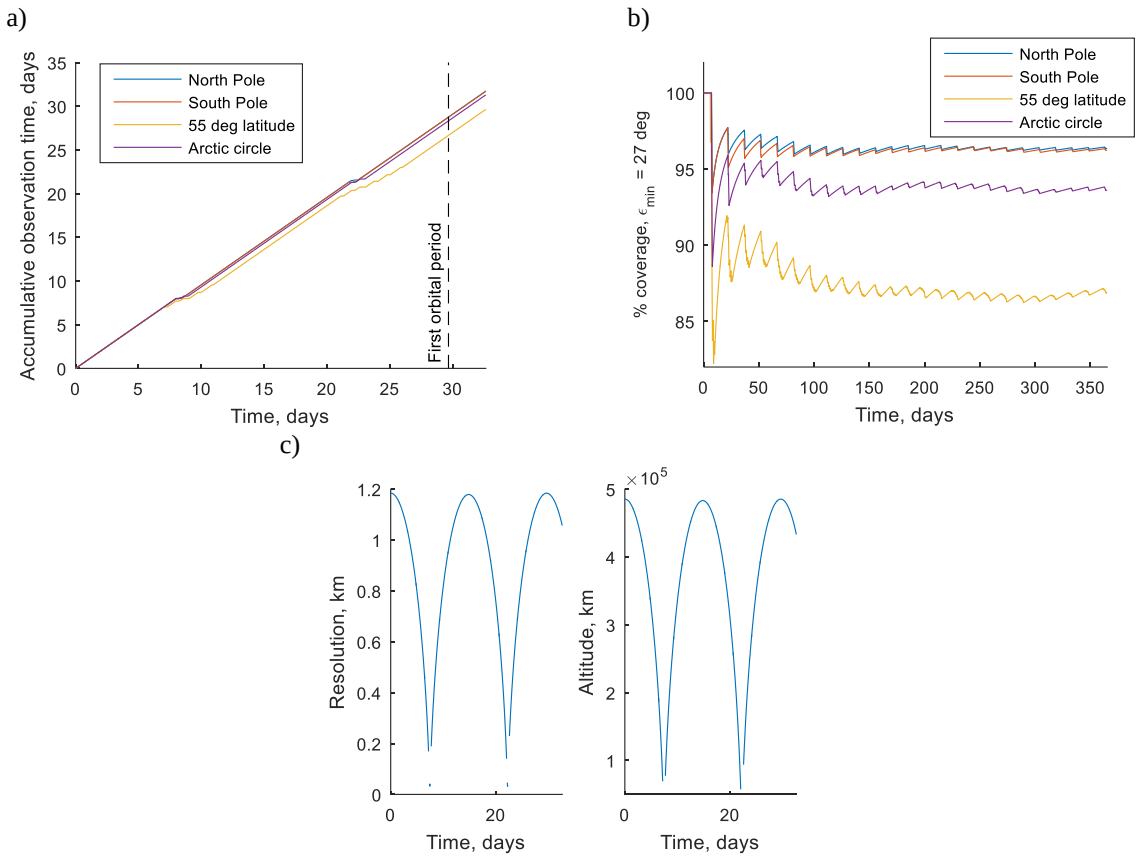

Figure 9 Clover-shaped orbits, constellation 2. a) Accumulative observation time over first orbit revolution. b) Percentage temporal coverage over time. c) Resolution and altitude (North Pole).

B. Vertical Lyapunov orbits for lunar observation

The far-side of the Moon has long held the interest of scientists and is considered as one of the possible locations for a future (permanent) human base. One of the most striking features on the far side of the Moon is the Aitken basin (coordinates of its center are 53°S 169°W), a huge impact crater which is believed to hold clues to the history of the Moon and allows access to the deeper layers of the lunar crust.[1] Regarding the human base, the lunar South Pole (in particular the rim of the Shackleton crater, 89.9°S 180°W) is often mentioned as a potential location as it is an area of near-permanent sunlight, providing access to power, and water ice may be present in the continuously shaded areas of the crater interior ([22], Chapter 4). For support of the occupants of the base, a continuous communication link with Earth will be essential, which is not guaranteed from the South Pole. Traditionally, natural halo orbits at L_2 are proposed to this end [23, 24], but a single spacecraft cannot provide sufficient coverage. Studies have therefore been conducted to use a combination of halo, vertical and butterfly families at the Earth-Moon L_1 and L_2 points, showing that several combinations of two of these orbits can achieve continuous coverage of the South Pole [25]. Other studies

[1] Lunar and Planetary Institute, Feasibility Assessment of All Science Concepts within South Pole-Aitken Basin, Accessed 31 July 2016

have investigated the use of a solar sail to maintain a non-Keplerian orbit below the South Pole to achieve continuous coverage and line-of-sight with the Earth with a single spacecraft [26, 27]. While all these studies focus on coverage of the South Pole only, the solar sail vertical Lyapunov orbits of Figure 4 will be investigated for continuous coverage of both the lunar South Pole *and* the center of the Aitken basin. Furthermore, compared to the solar sail trajectories below the South Pole presented in References [26, 27], which use an optimal steering law, the orbits in Figure 4 greatly simplify the steering of the sail through the assumed fixed solar sail attitude with respect to the Sun. Future investigations may furthermore provide a trade-off between these different concepts in terms of altitude, elevation angles, and so on.

Conducting similar analyses as shown in Section VI in Figure 5 leads to the selection of a particular constellation of two L_2 vertical Lyapunov orbits. Figure 10a and b show this constellation, which consists of one orbit with $a_{0,\mathrm{EM}} = 0.1$ and one with $a_{0,\mathrm{EM}} = 0.083$ (mirrored in the (x, y)-plane). In this case, a minimum elevation of $\varepsilon_{\mathrm{lim}} = 15$ deg is assumed in compliance with References [25-27]. The elevation profiles in Figure 10c and d then show that the constellation in subplot a) can achieve continuous coverage of both the South Pole and the Aitken Basin. Coverage of the rest of the Moon is reasonable, see Figure 10e, except for a spot around the lunar equator on the Earth-facing side of the Moon. Finally, information about the spatial resolution from and altitude of the constellation is shown in Figure 10f. Note that the figure shows the results for the South Pole only but that nearly identical results can be obtained for the center of the Aitken basin due to the relatively high altitude of the orbits. Finally, note that plots such as those provided for the Earth-centred orbits in Figure 7a, b and Figure 9a, b are omitted because continuous, i.e., 100 percent temporal coverage is achieved, which would result in straight lines in those kind of plots.

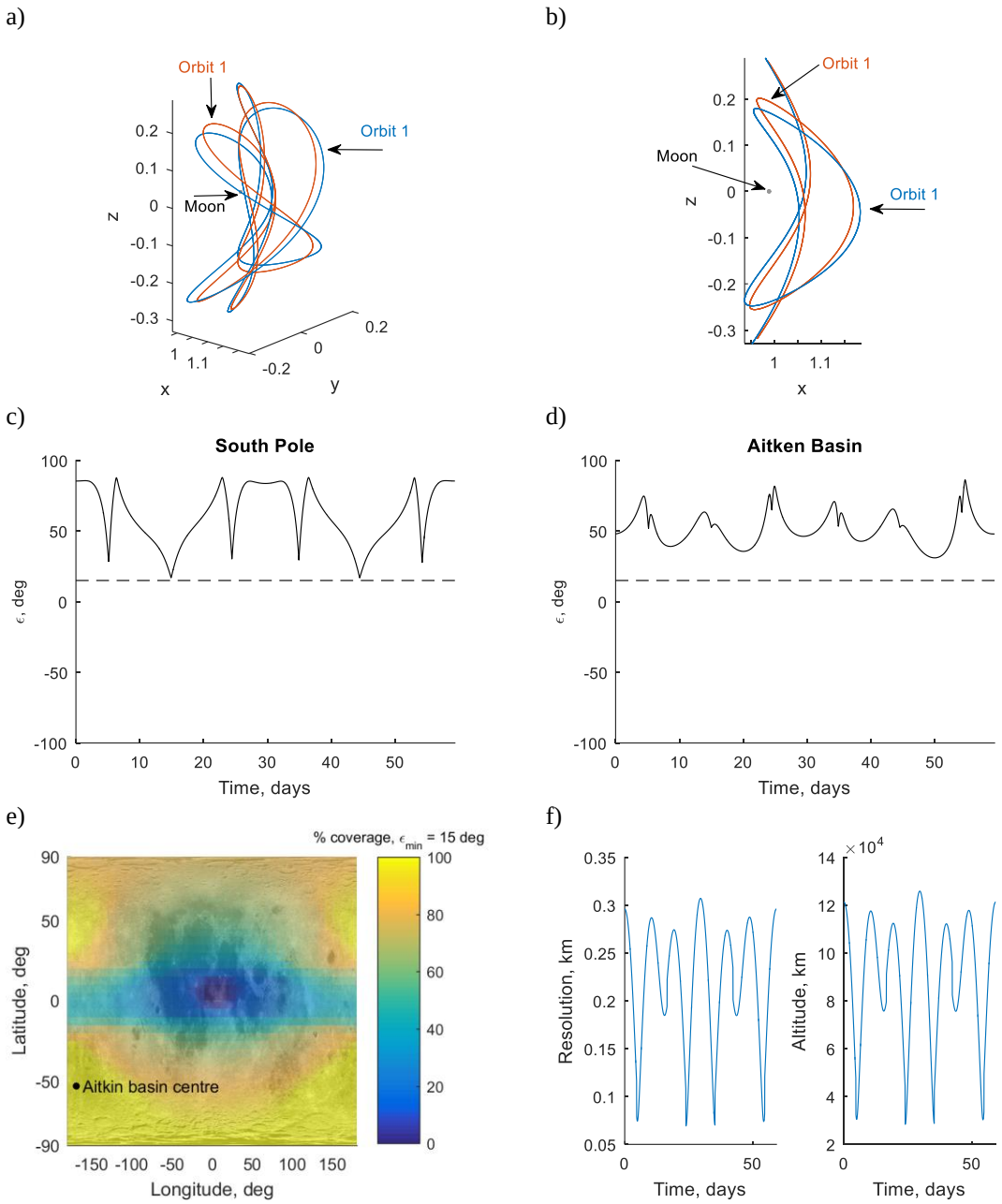

Figure 10 Constellation of solar sail L_2 vertical Lyapunov orbits. a,b) Constellation. c) Best elevation angle at lunar South Pole. d) Best elevation angle at center of Aitken Basin. e) Percentage temporal coverage for minimum elevation of 15 deg. f) Resolution and altitude (South Pole).

V. High-fidelity model

Because the constellations of orbits in the previous section have been designed within the framework of the circular restricted three-body problem and by neglecting the offset between the ecliptic and the Earth-Moon planes, further analyses are required to demonstrate that these orbits still hold in higher-fidelity models. Therefore, in this section,

the orbits of Section IV will be investigated taking the out-of-plane motion of the Sun and the eccentricity of the Moon into account.

A. Influence of out-of-plane motion of the Sun

The offset between the ecliptic plane and the Earth-Moon plane of $\delta_S = 5.145$ deg can be modelled through the Sun-vector, $\hat{\mathbf{S}}$, as follows (see Figure 11):

$$i_S = \delta_S \cos\left(\Omega_S t - \phi_S\right) \tag{5}$$

$$\hat{\mathbf{S}} = \left[\cos\left(i_S\right)\cos\left(\Omega_S t\right) \quad -\cos\left(i_S\right)\sin\left(\Omega_S t\right) \quad \sin\left(i_S\right)\right]^T \tag{6}$$

with $\phi_S = 0$ or $\phi_S = \pi$ the orientation of the ecliptic with respect to the Earth Moon plane, where $\phi_S = 0$ is the situation as depicted in Figure 11 (with the maximum out-of-plane position of the Sun along the $-x$-axis), while $\phi_S = \pi$ mirrors the Sun's orbit in the (x, y)-plane (maximum out-of-plane position of the Sun along the $+x$-axis). This Sun-vector feeds into the solar sail induced acceleration vector in Eq. (2) or (3). Note that, the effect of this offset between the ecliptic and Earth-Moon planes is a small (extra) out-of-plane solar sail acceleration component.

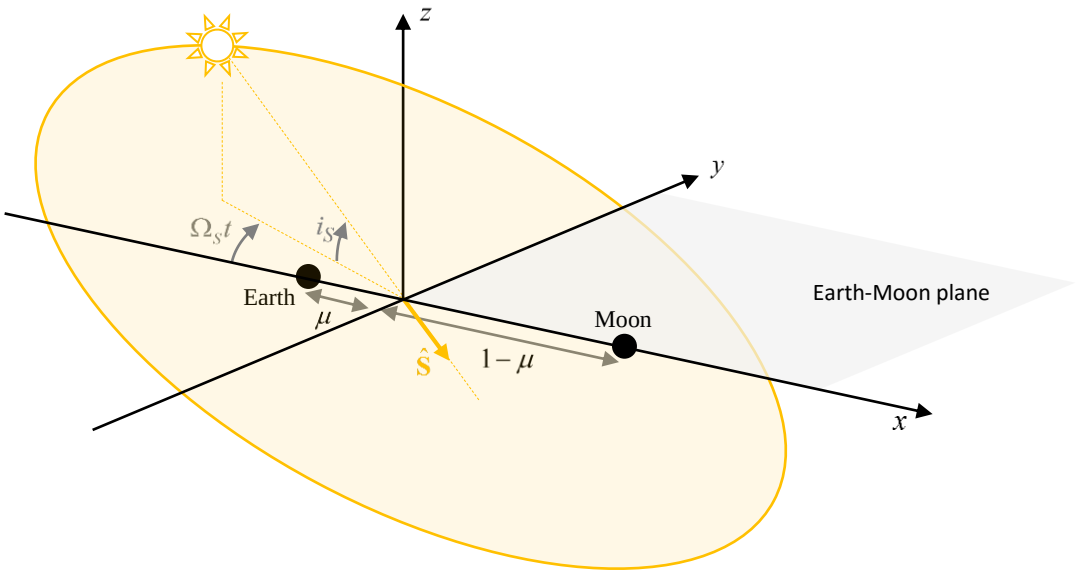

Figure 11 Schematic of offset between Earth-Moon plane and ecliptic plane.

New families of solar sail periodic orbits can be generated when taking the δ_S-offset into account using the same differential correction scheme and continuation approach as described in Section II. The result for the clover-shaped and out-of-plane vertical Lyapunov orbits presented in the previous section is shown in Figure 12. This figure shows

both the previous result (where the ecliptic and Earth-Moon planes are assumed to coincide: "Sun is in-plane") and the cases where $\phi_S = 0$ and $\phi_S = \pi$. The difference between the low- and high-fidelity model orbits is barely visible and remains small even if larger sail accelerations are considered (compare Figure 12a and b and Figure 12c and d). This is verified in Figure 13a, which shows the altitude of the spacecraft above the Earth or Moon for the orbits in Figure 12a and d, respectively. The difference between the altitudes is given in Figure 13b (which indeed shows only a few percent difference in altitude for the cases where the Sun's motion is considered to be in and out-of the Earth-Moon plane, respectively). Finally, Figure 13c provides the effect of the out-of-plane motion of the Sun on the linear stability of the orbit families, showing a slight destabilising effect for the clover-shaped orbits, but a further stabilizing effect for the vertical Lyapunov orbits.

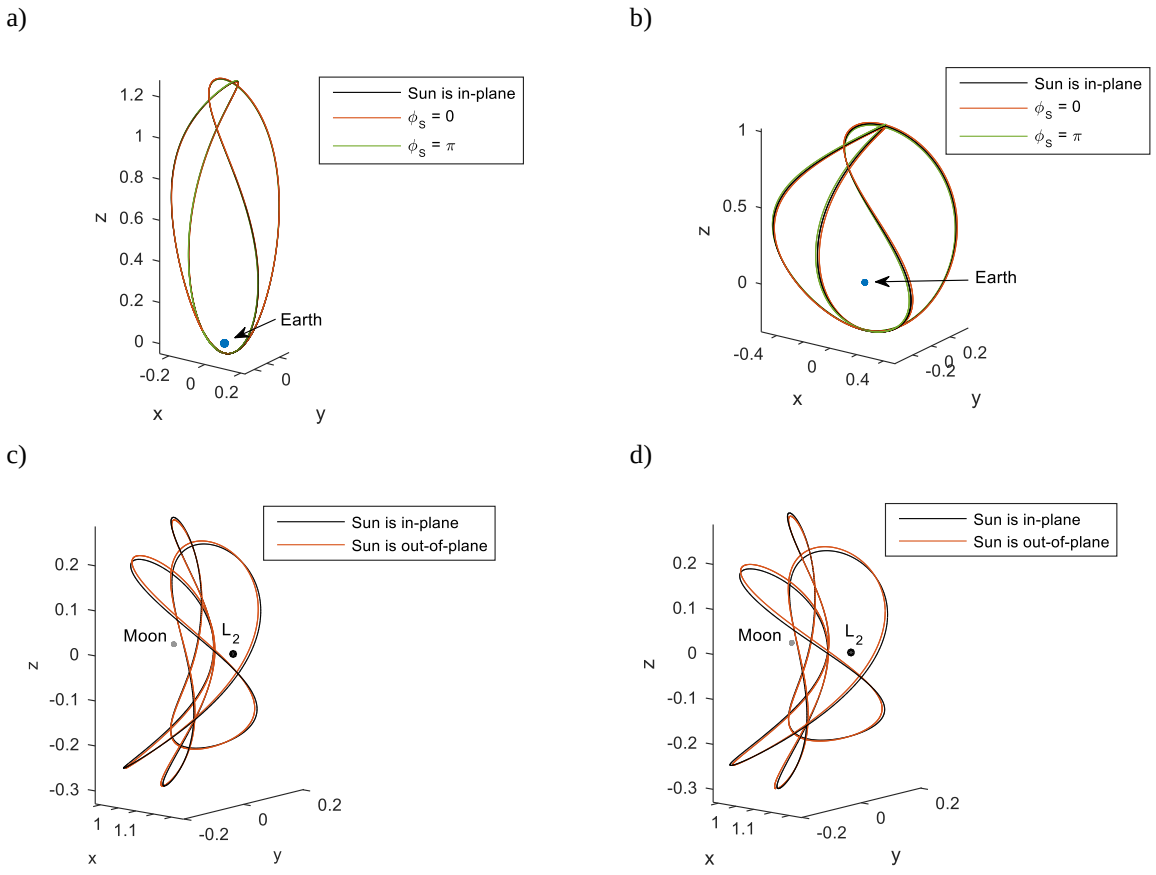

Figure 12 Effect of offset between Earth-Moon plane and ecliptic plane. a) Clover-shaped orbits with $a_{0,EM}$ = 0.025. b) Clover-shaped orbits with $a_{0,EM}$ = 0.1. c) Vertical Lyapunov orbits with $a_{0,EM}$ = 0.083. d) Vertical Lyapunov orbits with $a_{0,EM}$ = 0.1.

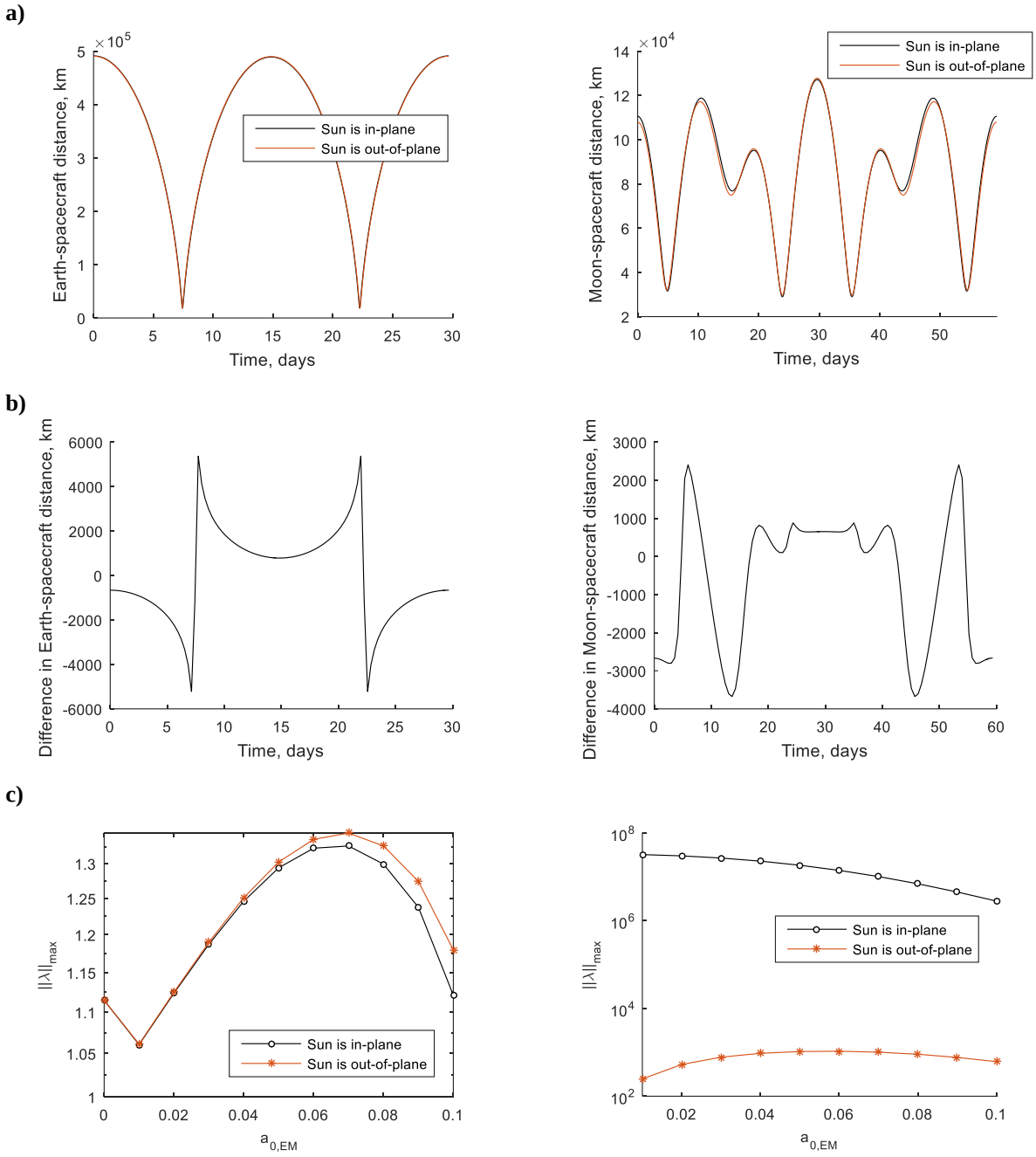

Figure 13 Details for effect of offset between Earth-Moon plane and ecliptic plane for orbits in Figure 12a (left column) and Figure 12d (right column). a) Distance to Earth or Moon for in-plane and out-of-plane cases. b) Difference in distance according to subplot a). c) Effect on stability of orbit family.

B. Effect of lunar eccentricity

To account for the eccentricity of the Moon, $e = 0.0549$, a multiple shooting differential correction scheme is implemented using the framework of the solar sail elliptic restricted three-body problem [28]:

$$
\begin{aligned}
X''-2Y' &= \frac{1}{1+e\cos\theta}\left(\frac{\partial\Omega}{\partial X}+a_{s,X}\right)\\
Y''+2X' &= \frac{1}{1+e\cos\theta}\left(\frac{\partial\Omega}{\partial Y}+a_{s,Y}\right)\\
Z''+Z &= \frac{1}{1+e\cos\theta}\left(\frac{\partial\Omega}{\partial Z}+a_{s,Z}\right)
\end{aligned}
\quad . \tag{7}
$$

The prime in Eq. (7) indicates the derivative with respect to the Moon's true anomaly, θ, and the solar sail state vector, $\mathbf{X}=\begin{bmatrix}X & Y & Z & X' & Y' & Z'\end{bmatrix}^T$ is defined in a pulsating rotating reference frame (such that the Earth and Moon are always located at $\mathbf{X}=\begin{bmatrix}1-\mu & 0 & 0\end{bmatrix}^T$ and $\mathbf{X}=\begin{bmatrix}-\mu & 0 & 0\end{bmatrix}^T$, respectively). The transformation required to get back to the traditional synodic reference frame coordinates, $\mathbf{x}(x,y,z)$ is: $\mathbf{x}=\frac{1-e^2}{1+e\cos\theta}\mathbf{X}$. Furthermore, in Eq. (7),

$$
\Omega=\frac{1}{2}\left(X^2+Y^2+Z^2\right)+\frac{1-\mu}{|\mathbf{r}_1|}+\frac{\mu}{|\mathbf{r}_2|} \tag{8}
$$

and $a_{s,X}$, $a_{s,Y}$ and $a_{s,Z}$ are the solar sail acceleration components in X-, Y- and Z-direction, respectively. In order to compute these acceleration components, which depend on the orientation of the Sun-vector in Eq. (6), the actual time (rather than the true anomaly) needs to be known, which can be computed following [29] as

$$
E=\tan 2^{-1}\left(\frac{\sqrt{1-e^2}\sin\theta}{e+\cos\theta}\right) \tag{9}
$$

$$
M=E-e\sin E \tag{10}
$$

$$
t=\mathrm{mod}\left(M,2\pi\right)+2\pi\times\mathrm{floor}\left(\frac{\theta}{2\pi}\right), \tag{11}
$$

where E, M and t are the eccentric anomaly, mean anomaly and dimensionless time, respectively.

In order to find solar sail periodic orbits within the dynamical framework of Eq. (7), a multiple shooting differential correction (MSDC) scheme is implemented, similar to the works in [30-32]. MSDC divides an initial guess of the trajectory into segments by defining patch points at appropriate locations. Here, the orbits in the *circular* restricted three-body problem are used as initial guess and a continuation scheme is applied to slowly increase the eccentricity of the Moon's orbit. The advantage of starting from an orbit (with associated time vector) that exists for $e=0$ is that the true anomaly is equal to the dimensionless time. This eliminates the transformation of the velocity and acceleration states from time units to angle units. Once the initial guess has been divided into segments, two differential correction 'levels' are applied to sequentially adjust the position of the patch points and the velocities at the patch points to find orbits that hold under the dynamics of Eq. (7).

C. Clover-shaped orbits

Applying the MSDC scheme to the orbit in Figure 12a with $\phi_S = 0$ results in the orbits shown in Figure 14. While Figure 14a shows the orbits in the pulsating reference frame (where the Earth and Moon are static along the *X*-axis), Figure 14b shows them in the traditional synodic reference frame (where the Earth and Moon move along the *x*-axis, but this movement is not significant enough for the Earth to be visible in Figure 14b). The orbit in black is the previously obtained result in the CR3BP (taking the out-of-plane motion of the Sun into account), while the orbits in blue are the result in the elliptic restricted three-body system. Note that the analyses are conducted over multiple revolutions of the clover-shaped orbits (14 orbits) to cover an entire year. This is required because the period of the Earth-Moon system and Sun around the Earth-Moon system are not commensurate, causing the pulsating nature of the Earth-Moon system and the position of the Sun to get "out of sync", leading to the quasi-periodic motion visible in Figure 14. The effect of the lunar eccentricity is clear, but the orbital shape does not break down under its influence. A similar conclusion can be drawn for the orbit in Figure 12b with $\phi_S = 0$, see Figure 15.

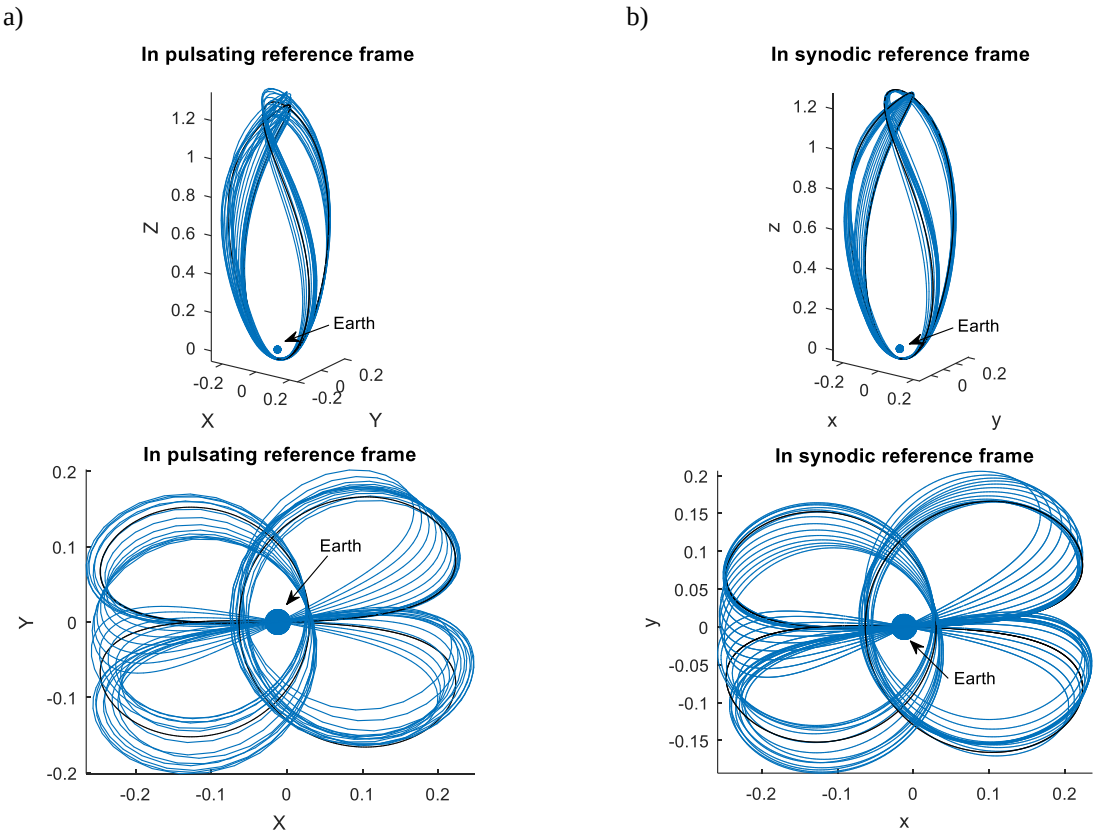

Figure 14 Effect of lunar eccentricity on the orbit of Figure 12a over one year with $\phi_S = 0$. Black and blue orbits are for $e = 0$ and $e = 0.0549$, respectively. a) In pulsating reference frame. b) In synodic CR3BP reference frame.

a) b)

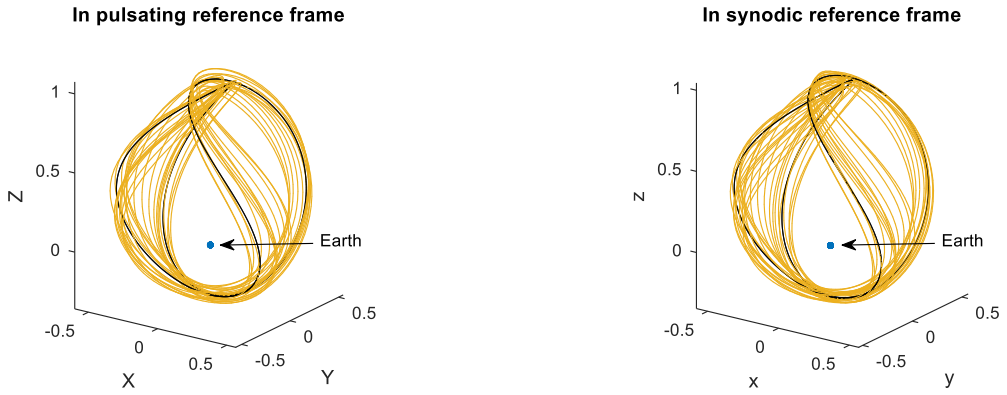

Figure 15 Effect of lunar eccentricity on the orbit of Figure 12b over one year with ϕ_S = 0. Black and yellow orbits are for *e* = 0 and *e* = 0.0549, respectively. a) In pulsating reference frame. b) In synodic CR3BP reference frame.

To assess the effect of the lunar eccentricity on the performance of these orbits for high-latitude coverage of the Earth, similar analyses as in Section IV.A are conducted and the overall results are provided in Table 2. Table 2 provides the temporal coverage of both the orbits in the low-fidelity model (i.e., the CR3BP, see also Table 1) and the high-fidelity model for the four latitudes previously considered in Section IV. Comparing the percentages shows that the out-of-plane motion of the Sun and the eccentricity of the Earth have only limited effect on the coverage. While for constellation 2 between 0 and 0.4 percent temporal coverage is lost, constellation 1 gains up to 0.5 percent temporal coverage.

Table 2 Percentage temporal coverage at different latitudes from clover-shaped orbits in low- and high-fidelity models for constellations 1 and 2.

Latitude	Constellation 1		Constellation 2	
	CR3BP	High-fidelity	CR3BP	High-fidelity
North Pole	99.6	99.5 (-0.1)	96.3	96.2 (-0.1)
South Pole	66.3	66.4 (+0.1)	96.3	96.3 (0.0)
Arctic circle	96.4	96.9 (+0.5)	93.7	93.5 (-0.2)
55 deg	89.1	89.4 (+0.3)	86.7	86.3 (-0.4)

D. Vertical Lyapunov orbits

Applying the MSDC scheme to the vertical Lyapunov orbits of Figure 12c and d provides the results as shown in Figure 16. Because the orbital period of the vertical Lyapunov orbits is equal to two lunar synodic months, seven orbital revolutions are shown in Figure 16 to cover the effect of the lunar eccentricity over a full year. Due to the closer proximity of the vertical Lypaunov orbits to the Moon, the effect of the lunar eccentricity is much greater than

what was observed for the Earth-centred clover shaped orbits in Figure 14 and Figure 15. Because the orbits in Figure 16 are presented in the synodic reference frame, also the motion of the Moon during the year becomes apparent (see the line of grey dots). Furthermore, although the plots in Figure 16a and b seem to suggest that the orbits and the motion of the Moon intersect, this is not the case. The minimum altitude of the constellation over time is 29,000 km. The performance of the constellation under high-fidelity dynamics for continuous observation of the center of the Aitken Basin and the South Pole is provided in Figure 16c and d. While the Aitken Basin remains visible for 100 percent of the time, the minimum elevation above the South Pole dips below the minimum required elevation of 15 deg, for a total of 2.5 days per year and to a minimum elevation angle of 9.5 deg.

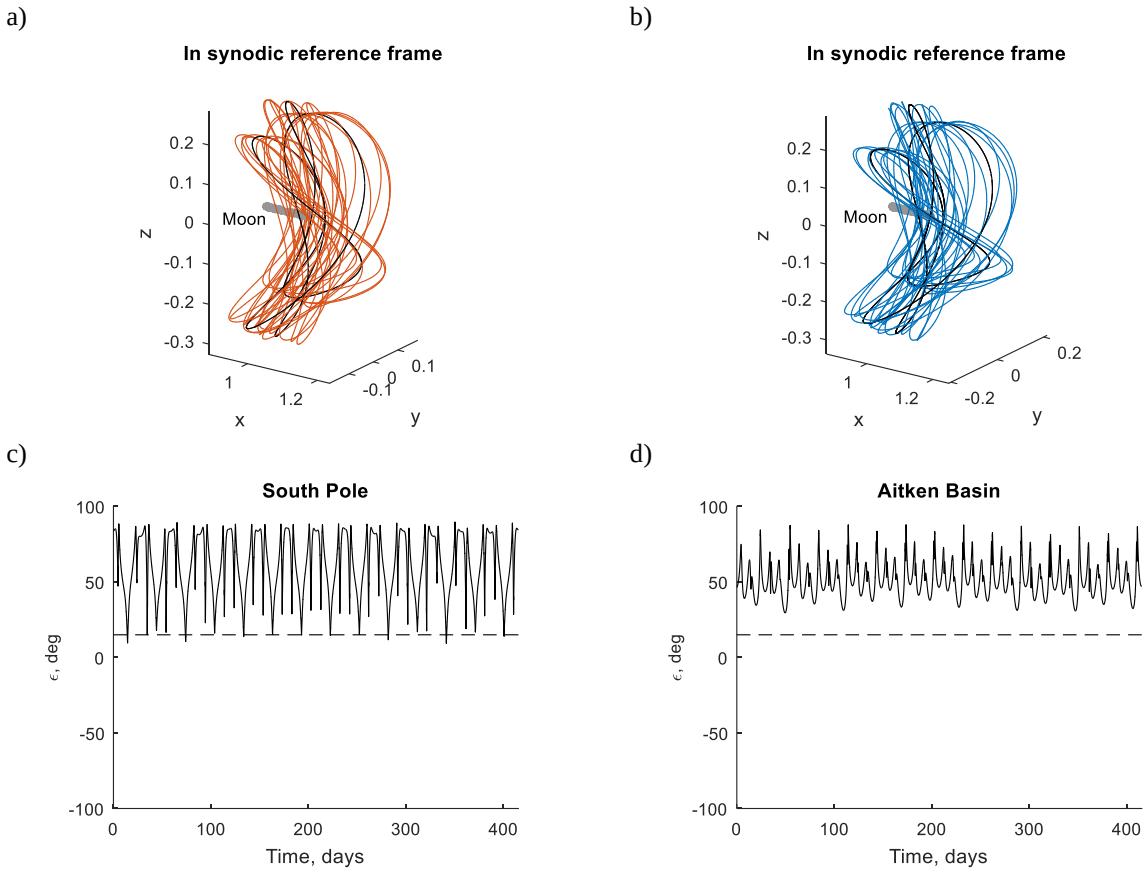

Figure 16 Effect of lunar eccentricity on the orbits of Figure 12c, d over one year with ϕ_S = 0. Black and coloured orbits are for *e* = 0 and *e* = 0.0549, respectively. a) For orbit of Figure 12c. b) For orbit of Figure 12d. c-d) Elevation of constellation over South Pole (c) and Aitken Basin (d).

Conclusions

This paper has introduced the novel family of clover-shaped, solar sail periodic orbits in the Earth-Moon circular restricted three-body problem (CR3BP) and evaluated a subset of orbits within this family for high-latitude observation of the Earth. From the observation analyses it follows that a constellation of two clover-shaped orbits can achieve near-continuous coverage of the North (or South) Pole (99.6 percent of the time) at a minimum elevation of $\varepsilon_{\text{lim}} =$

27 deg and continuous coverage of one of the Poles for $\varepsilon_{\lim} = 20$ deg. An alternative constellation of two clover-shaped orbits can achieve 96.3 percent temporal coverage of *both* Poles at $\varepsilon_{\lim} = 27$ deg (97.4 percent for $\varepsilon_{\lim} = 20$ deg). When transferring these orbits to a higher-fidelity model that takes the offset between the ecliptic and Earth-Moon planes into account as well as the lunar eccentricity, quasi-periodic orbits are achieved that oscillate around the nominal CR3BP orbits. It is shown that this quasi-periodic motion has only a very small impact on the observational capabilities of the orbits, showing a difference in the temporal coverage of between -0.4 and +0.5 percent, depending on the constellation and latitude considered.

The paper has also investigated the use of the previously introduced family of L_2 vertical Lyapunov orbits in the Earth-Moon system for simultaneous and continuous observation of the lunar South Pole and the center of the Aitken Basin at a minimum elevation of 15 deg. Again, it is shown that with an appropriate choice of two CR3BP orbits within this family, a continuous link with both targets can be established. Due to the closer proximity to the Moon, the effect of the lunar eccentricity is much greater than for the clover-shaped orbits, showing a greater offset between the orbits in the CR3BP and the high-fidelity model. While the center of the Aitken Basin is still continuously in view with elevation angles above the minimum required value of 15 deg, the elevation of the sailcraft at the South Pole dips below the minimum value for 2.5 days per year, down to an elevation of 9.5 deg.

Rather than allowing the periodic orbits in the CR3BP to become quasi-periodic under the influence of the eccentricity of the Moon, future work will investigate the possibility of orbital control, to track the nominal CR3BP orbits under the influence of the eccentricity of the Earth. Because the orbits in the CR3BP allowed continuous coverage of the lunar South Pole, this approach will ensure that also under high fidelity models this requirement is met.

Acknowledgements

Jeannette Heiligers would like to acknowledge the support of the Marie Skłodowska-Curie Individual Fellowship 658645 - S4ILS: Solar Sailing for Space Situational Awareness in the Lunar System.

References

1. McNutt, L., Johnson, L., Clardy, D., Castillo-Rogez, J., Frick, A., and Jones, L., "Near-Earth Asteroid Scout," *AIAA SPACE 2014 Conference and Exposition*, American Institute of Aeronautics and Astronautics, San Diego, CA, 2014.
2. McInnes, C.R., "Solar Sailing: Technology, Dynamics and Mission Applications," *Springer-Praxis Books in Astronautical Engineering*, Springer-Verlag, Berlin, 1999.
3. Vulpetti, G., Johnson, L., and Matloff, G.L., "Solar Sails A Novel Approach to Interplanetary Travel, 2nd Edition," *Springer-Praxis Books in Space Exploration*, 2nd ed., Springer Science+Business Media, New York, 2015.
4. Macdonald, M., McInnes, C., Alexander, D., and Sandman, A., "GeoSail: Exploring the Magnetosphere Using a Low-cost Solar Sail," *Acta Astronautica*; Vol. 59, 2006, pp. 757-767. doi: 10.1016/j.actaastro.2005.07.023
5. Macdonald, M. and McInnes, C., "Solar Sail Science Mission Applications and Advancement," *Advances in Space Research*; Vol. 48, No. 11, 2011, pp. 1702-1716. doi: 10.1016/j.asr.2011.03.018

6. McInnes, C.R., Macdonald, M., Angelopolous, V., and Alexander, D., "GEOSAIL: Exploring the Geomagnetic Tail Using a Small Solar Sail," *Journal of Spacecraft and Rockets*; Vol. 38, No. 4, 2001, pp. 622-629. doi: 10.2514/2.3727
7. Macdonald, M., Hughes, G., McInnes, C., A, L., Falkner, P., and Atzei, A., "GeoSail: An Elegant Solar Sail Demonstration Mission," *Journal of Spacecraft and Rockets*; Vol. 44, No. 4, 2007, pp. 784-796. doi: 10.2514/1.22867
8. West, J.L., "The GeoStorm Warning Mission: Enhanced Opportunities Based on New Technology," *14th AAS/AIAA Spaceflight Mechanics Conference*, AAS-04-102, Maui, Hawaii, 2004.
9. Heiligers, J., Diedrich, B., Derbes, B., and McInnes, C.R., "Sunjammer: Preliminary End-to-End Mission Design," *2014 AIAA/AAS Astrodynamics Specialist Conference*, San Diego, CA, USA, 2014.
10. Macdonald, M., Hughes, G.W., Mcinnes, C.R., Lyngvi, A., Falkner, P., and Atzei, A., "A Solar Sail Technology Reference Study," *Journal of Spacecraft and Rockets*; Vol. 43, 2006, pp. 960-972
11. Macdonald, M., McInnes, C., and Hughes, G., "Technology Requirements of Exploration Beyond Neptune by Solar Sail Propulsion," *Journal of Spacecraft and Rockets*; Vol. 47, No. 3, 2010, pp. 472-483. doi: 10.2514/1.46657
12. Gautier, D.L., Bird, K.J., Charpentier, R.R., Grantz, A., Houseknecht, D.W., Klett, T.R., Moore, T.E., Pitman, J.K., Schenk, C.J., Schuenemeyer, J.H., Sørensen, K., Tennyson, M.E., Valin, Z.C., and C.J., W., "Assessment of Undiscovered Oil and Gas in the Arctic," *Science*; Vol. 324, No. 5931, 2009, pp. 1175-1179. doi: 10.1126/science.1169467
13. Heiligers, J., Hiddink, S., Noomen, R., and McInnes, C.R., "Solar Sail Lyapunov and Halo Orbits in the Earth-Moon Three-Body Problem," *Acta Astronautica*; Vol. 116, 2015, pp. 25-35. doi: 10.1016/j.actaastro.2015.05.034
14. Heiligers, J., Macdonald, M., and Parker, J.S., "Extension of Earth-Moon Libration Point Orbits with Solar Sail Propulsion," *Astrophysics and Space Sciences, In Press*; Vol. 361 : 241, 2016. doi: 10.1007/s10509-016-2783-3
15. Battin, R.H., "An Introduction to the Mathematics and Methods of Astrodynamics, Revised Edition," *AIAA Eduction Series*, American Institute of Aeronautics and Astronautics, Inc., Reston, USA, 1999.
16. Howell, K.C., "Three-dimensional, periodic, 'Halo' orbits," *Celestial Mechanics*; Vol. 32, 1983, pp. 53-71. doi: 10.1007/BF01358403
17. Walmsley, M., Heiligers, J., Ceriotti, M., and McInnes, C., "Optimal Trajectories for Planetary Pole-Sitter Missions," *Journal of Guidance, Control, and Dynamics, Under Review*; Vol., 2016
18. Anderson, P. and Macdonald, M., "Extension of Highly Elliptical Earth Orbits Using Continuous Low-Thrust Propulsion," *Journal of Guidance, Control, and Dynamics*; Vol. 36, No. 1, 2013, pp. 282-292. doi: 10.2514/1.55304
19. Ceriotti, M., Heiligers, J., and McInnes, C.R., "Trajectory and Spacecraft Design for a Pole-Sitter Mission," *Journal of Spacecraft and Rockets*; Vol. 51, No. 1, 2014, pp. 311-326. doi: 10.2514/1.A32477
20. Waters, T.J. and McInnes, C.R., "Periodic Orbits Above the Ecliptic in the Solar-Sail Restricted Three-Body Problem," *Journal of Guidance, Control, and Dynamics*; Vol. 30, No. 3, 2007, pp. 687-693. doi: 10.2514/1.26232
21. Ceriotti, M. and McInnes, C., "Natural and sail-displaced doubly-symmetric Lagrange point orbits for polar coverage," *Celestial Mechanics and Dynamical Astronomy*; Vol., 2012. doi: 10.1007/s10569-012-9422-2
22. National Aeronautics and Space Administration (NASA), "NASA's Exploration Systems Architecture Study (NASA-TM-2005-214062)," 2005.
23. Farquhar, R.W., "The Utilization of Halo Orbits in Advanced Lunar Operations, NASA TN D-6365," Washington, D.C., 1971.
24. Farquhar, R.W., "A Halo-Orbit Lunar Station," *Astronautics & Aeronautics*; Vol., 1972, pp. 59-63
25. Grebow, D.J., Ozimek, M.T., and Howell, K.C., "Multibody Orbit Architectures for Lunar South Pole Coverage," *Journal of Spacecraft and Rockets*; Vol. 45, No. 2, 2008, pp. 344-358. doi: 10.2514/1.28738
26. Wawrzyniak, G.G. and Howell, K.C., "Investigating the Design Space for Solar Sail Trajectories in the Earth-Moon System," *The Open Aerospace Engineering Journal*; Vol. 4, 2011, pp. 26-44
27. Wawrzyniak, G.G. and Howell, K.C., "Generating Solar Sail Trajectories in the Earth-Moon System Using Augmented Finite-Difference Methods (Article ID 476197)," *International Journal of Aerospace Engineering*; Vol., 2011. doi: 10.1155/2011/476197
28. Biggs, J.D., McInnes, C.R., and Waters, T., "Control of Solar Sail Periodic Orbits in the Elliptic Three-Body Problem," *Journal of Guidance, Control, and Dynamics*; Vol. 32, No. 1, 2009, pp. 318-320. doi: 10.2514/1.38362

29. Wertz, J.R., "Mission Geometry; Orbit and Constellation Design and Management," Space Technology Library, Microcosm Press/Kluwer Academic Publishers, El Segundo, USA/London, UK, 2001.
30. Parker, J.S. and Anderson, R.L., "Low-Energy Lunar Trajectory Design," *Deep Space Communications and Navigation Series*, Jet Propulsion Laboratory, Pasadena, California, USA, 2013.
31. Howell, K.C. and Pernicka, H.J., "Numerical Determination of Lissajous Trajectories in the Restricted Three-Body Problem," *Celestial Mechanics*; Vol. 41, 1988, pp. 107-124
32. Marchand, B.G., Howell, K.C., and Wilson, R.S., "Improved Corrections Process for Constrained Trajectory Design in the n-Body Problem," *Journal of Spacecraft and Rockets*; Vol. 44, No. 4, 2007, pp. 884-897